

UNCLASSIFIED

Defense Technical Information Center Compilation Part Notice

ADP010722

TITLE: Wing and FIN Buffet on the Standard
Dynamics Model

DISTRIBUTION: Approved for public release, distribution unlimited

This paper is part of the following report:

TITLE: Verification and Validation Data for
Computational Unsteady Aerodynamics [Donnees de
verification et de valadation pour
l'aerodynamique instationnaire numerique]

To order the complete compilation report, use: ADA390566

The component part is provided here to allow users access to individually authored sections of proceedings, annals, symposia, ect. However, the component should be considered within the context of the overall compilation report and not as a stand-alone technical report.

The following component part numbers comprise the compilation report:

ADP010704 thru ADP010735

UNCLASSIFIED

15E. WING AND FIN BUFFET ON THE STANDARD DYNAMICS MODEL

Reported by X. Z. Huang
of work by S. Zan et al.
IAR/NRC, Canada

INTRODUCTION

For modern aircraft with higher sweep angles flying at higher incidence, unsteady and burst vortex flow in the vicinity of the wing and downstream lifting surface lead to strong unsteady airloads and buffeting¹. Thus, investigations were conducted in the Institute for Aerospace Research (IAR) Low Speed Wind Tunnel (LSWT)² to study the buffet characteristics of the Standard Dynamics Model (SDM)³, a generic fighter aircraft configuration.

Since the spectrum of the aerodynamic input load is reasonably flat over the frequency range of interest, the solution to the equation of the motion is easily solved in the frequency domain for a given aerodynamic loads and vice versa. Following Jones⁴ and Mabey⁵, it is suggested that $\sqrt{nG(n)}$ is the best parameter to use as a measure of buffet excitation due to flow separations and unsteadiness and to denote this as the buffet excitation parameter.

Buffeting is presented for three modes – the fin bending mode (VFB) and the wing symmetric and anti-symmetric bending modes (WSB and WAB)⁶. The strain gauges were mounted approximately on the node line of the torsional mode. It should be emphasized that since the model is rigid and the deformation of the structure and its damping are negligible, this measurement is linearly related to the buffet excitation. In addition, experimental results of static coefficients at angles of attack ranging from 0° to 90° are also included⁷ for the understanding of the flow behavior during the experiments.

The geometry of SDM is shown in Fig. 1. There are two SDM models with ratio of 0.375 (SDM-L and SDM-S) used for buffet/dynamic stability and static experiments respectively.

The SDM model was sting-mounted in the wind tunnel⁸, which in turn was protruded from a strut cantilevered in the wind tunnel floor as shown in Fig. 2 and Fig. 3. The pitch angle is obtained by turning the strut through the center of the turntable. Sideslip angle setting is effected by banking the model about the body axis.

The flow visualization results show that at $\beta = 0^\circ$, separation becomes evident on the wing at $\alpha \approx 4^\circ$ in the case of strakes removed and $\alpha \approx 15^\circ$ in the case of strakes installed. At $\alpha \approx 20^\circ$, the vortex burst reaches the wing trailing edge while it breaks down completely over the wing at $\alpha \approx 29^\circ$. The onset of asymmetrical forebody vortices appears at $\alpha \approx 40^\circ$.

The test matrix for the buffet characteristics is presented in Table 1. The experimental results of static coefficients and buffet characteristics at different conditions are listed in Table 2 and Table 3 in the CD-ROM and illustrated from Fig. 4 to Fig. 6 and Fig. 10 to Fig. 14 respectively. The reference center for the moment is at 35% of MAC. The results with a dummy strut which was installed on the tunnel ceiling to investigate the asymmetrical effect of the strut are shown in Fig. 10 (cont.). In addition, Fig. 7 to Fig. 9 shows the shapes of different modes for the purpose of locating the strain gauges.

In general, the level of fin buffeting exceeds that of wing buffeting by an order of magnitude. In connecting with static measurements and flow visualizations this severe fin buffeting arises from the fact that the fin is immersed in the wake of the burst of strake and/or forebody vortices. The peak of fin buffet excitation is near an angle of attack corresponding to the onset of asymmetrical forebody flow. The magnitude of the wing buffet excitation parameter did not exceed 0.003, which arose from the interaction of the strake and wing vortices or simply from separated flow unsteadiness over the wing.

LIST OF SYMBOLS AND DEFINITIONS

B	wingspan (m)
\bar{c}	wing mean aerodynamic chord (MAC, m)
C_l	rolling moment coefficient ($=l/q_s B$)
C_m	pitching moment ($=m/q_s \bar{c}$)
C_n	yawing moment ($=n/q_s B$)
C_Y	side force coefficient ($=Y/q_s$)
C_Z	normal force coefficient ($=Z/q_s$)

d	body diameter at base (m)
d_r	ratio of diameters ($=d_s/d$)
d_s	sting diameter (m)
f	frequency (Hz)
f_0	modal frequency (Hz)
ℓ, m, n	rolling, pitching and yawing moment around body axes system
m	mode generalized mass
n	reduced frequency parameter ($=f \bar{c} / U_\infty$)
$\sqrt{nF(n)}$	unsteady pressure fluctuations
$\sqrt{nG(n)}$	buffet excitation parameter due to flow separations and flow unsteadiness
q	free stream dynamic pressure (N/m^2)
$F(n)$	non-dimensional power spectral density of unsteady pressure fluctuations
$G(n)$	non-dimensional power spectral density of excitation
Re_D	Reynolds number based on ogive base diameter
SDM	Standard Dynamics Model
s	wing area (m^2)
Stks	strakes
U_∞	free-stream velocity (m/sec)
VFB	vertical fin bending mode (376 Hz)
WAB	wing anti-symmetric bending mode (319 Hz)
WSB	wing symmetric bending mode (276 Hz)
X, Y, Z	axial, side and normal force around body axes system
α	angle of attack (deg)
β	angle of sideslip (deg)
θ	amplitude (deg)
σ	aerodynamic pitch angle (deg)
ϕ	roll angle (deg)
ω	circular frequency (rad/sec)

FORMULARY

1 General Description of model

1.1	Designation	Standard Dynamics Model (SDM)
1.2	Type	Full model
1.3	Derivation	F-16
1.4	Additional remarks	Interchangeable strakes (LEX)
1.5	References	Ref. 3

2 Model Geometry

2.1	Wing	
2.1.1	Planform	Cropped delta wing

2.1.2	Aspect ratio	3.0
2.1.3	Dihedral angle	0°
2.1.4	Leading edge sweep	40°
2.1.5	Trailing edge sweep	0°
2.1.6	Taper ratio	0.227
2.1.7	Twist	0°
2.1.8	Wing centerline chord	0.3310 m (SDM-L)
2.1.9	Wing tip chord	0.0752 m (SDM-L)
2.1.10	Wing span	0.6096 m (SDM-L)
2.1.11	Mean aerodynamic chord	0.2299 m (SDM-L)
2.1.12	Area of planform	0.1238 m ² (SDM-L)
2.1.13	Form of wing-body junction	With an interchangeable strakes (LEX)
2.1.14	Location of reference sections and definition of profiles	Double wedged with 4.5% at the root chord
2.1.15	Lofting procedure between reference sections	Linear taper
2.1.16	Lead-edge bevel	15° on both sides
2.1.17	Trailing edge bevel	15° on both sides
2.1.18	LEX angle	Double sweep back angles (73° and 83°)
2.1.19	Form of wing tip	Free stream aligned
2.2	Fuselage	
2.2.1	Length	0.9429 m (SDM-L)
2.2.2	Diameter at base	0.1347 m (SDM-L)
2.2.3	Fineness ratio	7
2.2.4	Nose	Tangent ogive
2.2.5	Fineness ratio of nose	3
2.2.6	Semi-apex angle of nose	18.92°
2.3	Horizontal stabilizer	
2.3.1	Planform	Cropped delta wing
2.3.2	Aspect ratio	1.88
2.3.3	Taper ratio	0.2126
2.3.4	Dihedral angle	-10°
2.3.5	Leading edge sweep	40°
2.3.6	Trailing edge sweep	0°
2.3.7	Lead-edge bevel	14°
2.3.8	Trailing edge bevel	15°
2.3.9	Twist	0°
2.3.10	Full span	0.3548 m (SDM-L)
2.3.11	Area of planform	0.06697 m ² (SDM-L)
2.3.10	Centre line chord	0.1919 m (SDM-L)
2.3.12	Tip chord	0.0408 m (SDM-L)
2.3.13	Location of reference sections and definition of profiles	Double wedged with 6.3% at the root chord
2.3.14	Lofting procedure between reference sections	Linear taper

2.3.15	Form of stabilizer -body junction	Fillet
2.3.16	Form of tip	Free stream aligned
2.4	Vertical stabilizer	
2.4.1	Planform	Trapezoid
2.4.2	Taper ratio	0.53
2.4.3	Leading edge sweep	47.5°
2.4.4	Trailing edge sweep	61.8°
2.4.5	Twist	0°
2.4.6	Height	0.1472 m (SDM-L)
2.4.7	Area of planform	0.01840 m ² (SDM-L)
2.4.8	Form of stabilizer -body junction	Fillet
2.4.9	Form of tip	Free stream aligned
2.5	Ventral fin	
2.1	Platform	Cropped trapezoid with LEX
2.2	Area of platform	0.003406 m ² (SDM-L)
2.3	Height	0.0481 m (SDM-L)
2.4	Leading-edge sweep	30°
2.5	Trailing edge sweep	0°
2.6	Reference	Detail drawings (Ref. 3) can be provided on the request

3 Wind Tunnel

3.1	Designation	IAR 6ft x 9ft low speed wind tunnel
3.2	Type of tunnel	Continuous atmospheric with closed return circuit
3.3	Test section dimensions	Height: 6 ft, width: 9ft, length: 15 ft
3.4	Type of roof	Solid with large optical quality plexiglass
3.5	Type of floor	Solid with turn table
3.6	Type of side walls	Solid with large optical quality plexiglass windows
3.7	Maximum speed	390 ft/sec
3.8	Contraction ratio	9
3.9	Support	Sting attached to wind tunnel strut (see Fig. 2 and Fig. 3)
3.10	Turbulence in empty tunnel	≤ 0.12% at free stream speed of 100 ft/sec
3.11	Acoustic noise in working section ($\sqrt{nF(n)}$)	≤ 0.0028
3.12	Mean flow angularity	± 0.1°
3.13	Wind tunnel acoustic resonance	The resonance of 416 and 475 Hz were eliminated before the buffet experiments
3.14	Velocity variation	± 0.25% at free-stream speed of 27.4 m/s
3.15	Variation in total ad static pressure	± 0.5% at free-stream speed of 27.4 m/s
3.16	References on tunnel	Ref. 2

4 Model motion (SDM-L)

4.1	General description	High natural frequency model mounted on the support with a large mass/low stiffness support
4.2	Model properties for three relevant modes	
4.2.1	Generalised mass (grams)	WSB=124, WAB=152, VFB=20.4
4.2.2	Characteristic area (m ²)	WSB=0.083, WAB=0.083, VFB=0.01459

4.2.3	First bending frequency (Hz)	WSB=276, WAB=319, VFB=377
4.3	Mode shapes	
4.3.1	Single wing	See Fig. 7
4.3.2	Vertical fin	See Fig. 8
4.3.3	Complete model modes	See Fig. 9

5 Test Conditions

5.1	Model planform area/tunnel area	0.0357 (SDM-L)
5.2	Model span/tunnel height	0.333 (SDM-L)
5.3	Blockage	Function of angle of attack
5.4	Position of model in tunnel	Standard side position
5.5	Range of velocities	25 m/s to 110 m/s for obtain different non-dimensional frequency.
5.6	Range of tunnel static pressure	Close to atmospheric pressure
5.7	Range of tunnel total temperature	Room temperature
5.8	Range of model steady or mean incidence	0° to 54°
5.9	Definition of model incidence	Angle between free-stream velocity vector and body axis in model's symmetric planform plane.
5.10	Position of transition, if free	N/A
5.11	Position and type of trip, if transition fixed	Two devices were used on the forebody: 1) A thin circumferential ring of adhesive tape fixed around the nose approximately 1.5 cm from the apex. 2) Two strips of #80 grit with 1.5 mm wide located on the windward side of the forebody at $\phi=\pm 40^\circ$ extended from apex to within 2 cm of the intake
5.12	Flow instabilities during tests	± 0.3 m/s
5.13	Model deformations	Negligible
5.14	References describing tests	Ref. 6, 7, 8

6 Measurements and Observations

6.1	Steady pressures for the mean conditions	Yes
6.2	Quasi-steady pressures	-
6.3	Unsteady pressures	-
6.4	Steady aerodynamic loads	Yes
6.5	Dynamic derivatives	Available but not included
6.6	Power spectral density of excitation	Yes
6.7	Buffet excitation parameter	Yes
6.8	Oscillation frequency	Yes
6.9	Single wing mode shapes	Yes (fundamental bending, torsion and overtone bending modes)
6.10	Fin mode shapes	Yes (bending and torsion modes)
6.11	Complete model modes	Yes (WSB, WAB and VFB modes)
6.12	Visualisation of surface flow	Yes but not included
6.13	Comparisons between free and fixed transition	Yes
6.14	Comparisons between strakes on and off	Yes

7 Instrumentation

7.1	Steady loads (SDM-S)	
7.1.1	Type of transducers	Strain gauges.
7.1.2	Type of measuring system	Six components balance (TASK balance)
7.1.3	Range of measuring system	Forward normal force $Z_1=445$ N

	Aft normal force $Z_2=445$ N
	Forward side force $Y_1=133$ N
	Aft side force $Y_2=133$ N
	Rolling moment $L=5.65$ N-m
	Axial force $X=133$ N
7.1.4 Method of calibration	Static calibration was performed on in situ in the wind tunnel
7.1.5 Principle and accuracy of calibration including interaction and temperature effect	$\leq 1\%$ of full-load output
7.2 Buffet excitation measurement	
7.2.1 Range of angle of attack	0° to 54°
7.2.2 Type of analysis	Measuring buffet excitation parameter, $\sqrt{nG(n)}$ obtained from the output of strain gauge bridges
7.2.3 Method of measurements	Strain gauges mounted approximately on the node line of the torsional mode (about 74% root chord of the wing and 37% root chord of the vertical tail).
7.2.4 Method of acquiring and processing measurement about wing buffet	Four gauges near the leading-edge were used to detect the symmetric bending mode and another four gauges aft were used to detect the anti-symmetric bending mode.
7.2.5 Method of acquiring and processing measurement about fin buffet	Four gauges near the leading-edge to detect the fin bending mode.
7.2.6 Sample rates	5500 Hz for the data channel of WSB mode and 7000 Hz for the channels of WAB and VFB modes
7.2.7 Windowing techniques	A Hanning window was used
7.2.8 Frequency range over which analysis is valid	WSB mode: $0.58 < n < 1.28$; WAB mode: $0.66 < n < 1.47$; VFB mode $0.96 < n < 1.73$
7.2.9 A/D conversion details	12 bit A/D, 32k samples per condition. Anti-aliasing filters were used with a cut-off frequency of 2500 Hz for the WSB channel and 3500 Hz for the WAB and VFB channels
7.3 References on techniques	See Ref. 6, 7

8 Data presentation

8.1 Test cases for which data could be made available	See Table 1
8.2 Test cases for which data are included in this document	See Table 1
8.3 Steady forces or moments	See Fig. 4 to Fig. 6 and Table 2 in CD ROM
8.4 Quasi-steady or unsteady perturbation forces	N/A
8.5 Buffet excitation	See Fig. 10 to Fig. 14 and Table 3 in CD ROM
8.6 Other forms in which data could be made available	N/A

9 Comments on data

9.1 Accuracy	-
9.1.1 Mach number	$\pm 0.1\%$ of set speed
9.1.2 Steady incidence	$\pm 0.01^\circ$
9.1.3 Reduced frequency	-
9.1.4 Steady aerodynamic loads coefficients	$\leq 1\%$ of full-load output
9.2 Influence of tunnel total pressure	Not examined
9.3 Effects on data of uncertainty, or	-

	variation, in mode of model motion	
9.4	Wall interference corrections	Following standard procedures the dynamic pressure was corrected for solid blockage and corrections were applied to the angle of attack to account for upwash caused by the tunnel walls
9.5	Wake blockage corrections	The correction to dynamic pressure due to wake blockage is $\leq 1\%$ and was not corrected for
9.6	Other relevant tests on same model	Dummy strut tests was conducted and found the support interference effects were small
9.7	Relevant tests on other models of nominally the same shapes	-
9.8	Any remarks relevant to comparison between experiment and theory	-
9.9	References on discussion of data	Ref. 6, 7

10 Personal contact for further information

Xing Zhong Huang, Aerodynamics Laboratory, Institute for Aerospace Research, National Research Council of Canada Building M-10, 1500 Montreal Rd. Ottawa, Ontario, Canada. K1A 0R6
e-mail xingzhong.huang@nrc.ca

11 List of references

1. Edwards, J.W., "Unsteady Airloads Due to Separated Flow on Airfoils and Wings," AGARD-CP-483.
2. Brown, T.R., "Description of the 6 ft x 9 ft Low Speed Wind Tunnel," NRC, NAE LTR-LA-285, Nov. 1986.
3. Huang, X.Z., "Standard Dynamics Model," T87-277-U, 1987.
4. Jones, J.G. "A Survey of the dynamic Analysis of Buffering and Related Phenomena," RAE TR 72197, 1973.
5. Mabey, D.G., "Some Aspect of Aircraft Dynamic Loads Due to Flow Separation," AGARD-R-750
6. Zan, S.J., "Measurements of Wing and Fin Buffeting on the Standard Dynamics Model," NRC No. 32158, IAR-AN-76, 1993.
7. Huang, X.Z. and Beyers, M.E., "Subsonic Aerodynamic Coefficients of the SDM at Angles of Attack up to 90° ," NAE LTR-UA-93, 1990.
8. Hansen, K., "Installation of Models in the 6 ft x 9 ft Low Speed Wind Tunnel," NAE LTR-LA-286, Aug. 1986.

Table 1 Test matrix of wing and fin buffet experiments (SDM-L)

U_∞	α°	β°	Strakes	Transition	Dummy strut	Data (Run number) in CD-ROM
50,70,90	$0 \leq 39$	0	On	No	No	104,105,106
110	$0 \leq 25$	0	On	No	No	107
70	$0 \leq 39$	$\pm 5, \pm 10$	On	No	No	108,109,110,111
50,70,90	$0 \leq 39$	0	On	fixed	No	113,114,115
50,70	20,29	0	On	fixed	Yes	116,117
70	20	$0, \pm 5$	On	No	Yes	118
50	20,29	0	On	No	Yes	119
110	$11 \leq 14$	0	On	fixed	No	122
50,70,90,	$0 \leq 39$	$0, \pm 5, \pm 10$	Off	No	No	156,157,158,161,162,163,164
50,70,90	$0 \leq 39$	0	Off	fixed	No	166,167,168
50,70	20,29	0	Off	fixed	Yes	169,170
50	20	$0, \pm 5$	Off	No	Yes	171
70	20,29	0	Off	No	Yes	172
70	24,30,36	$-10 \leq 10$	Off	No	No	173,174,175
60,70	$35 \leq 53$	$0, 5, 10$	On	No	No	200,201,202
70	42	$-10 \leq 10$	On	No	No	203
70	$35 \leq 53$	0	On	fixed	No	204
70	$35 \leq 53$	0	Off	fixed	No	205
70	$35 \leq 53$	$0, 5, 10$	Off	No	No	206,207,208
70	42	$-10 \leq 10$	Off	No	No	209

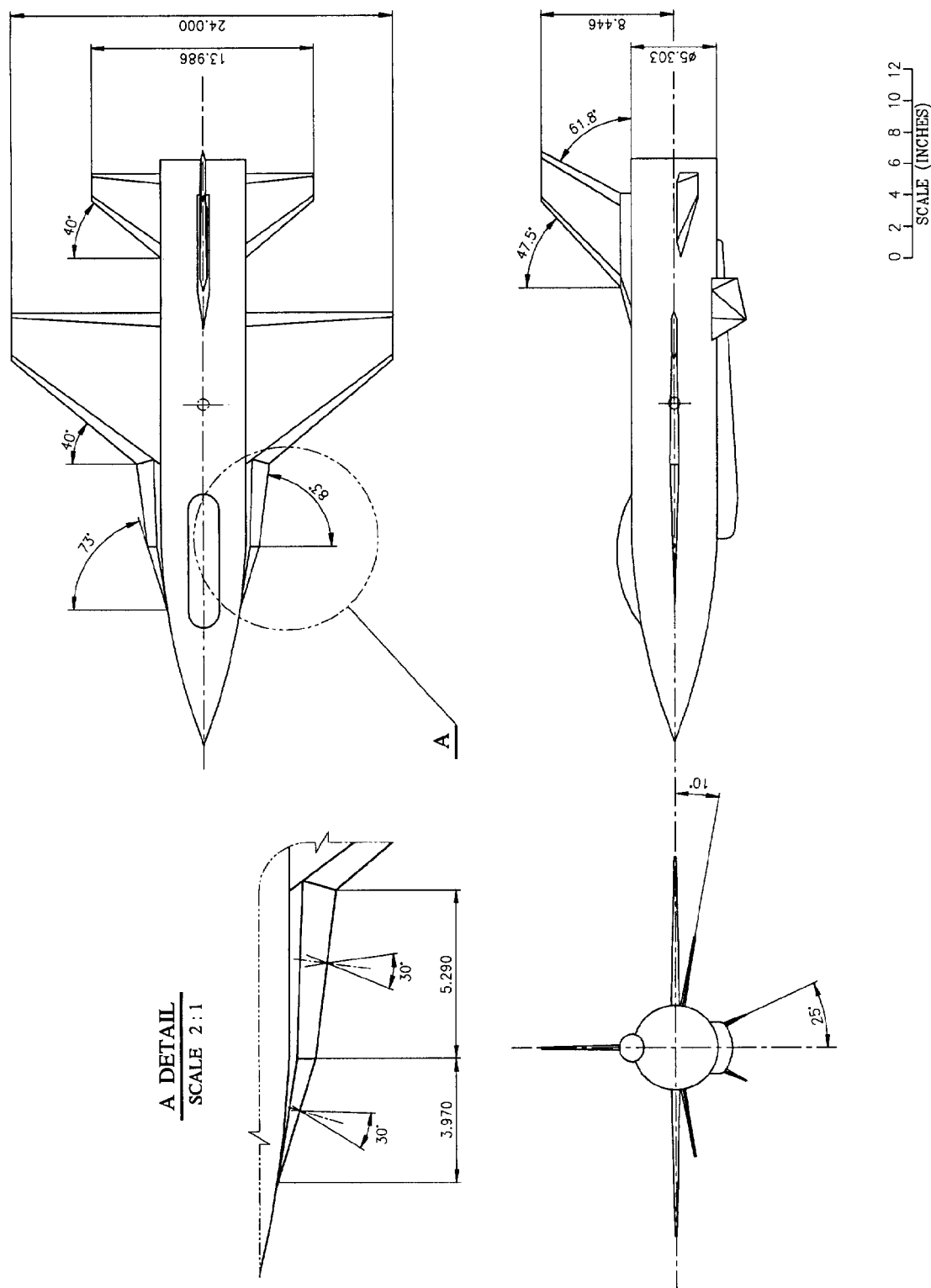


Fig. 1 Standard Dynamics Model

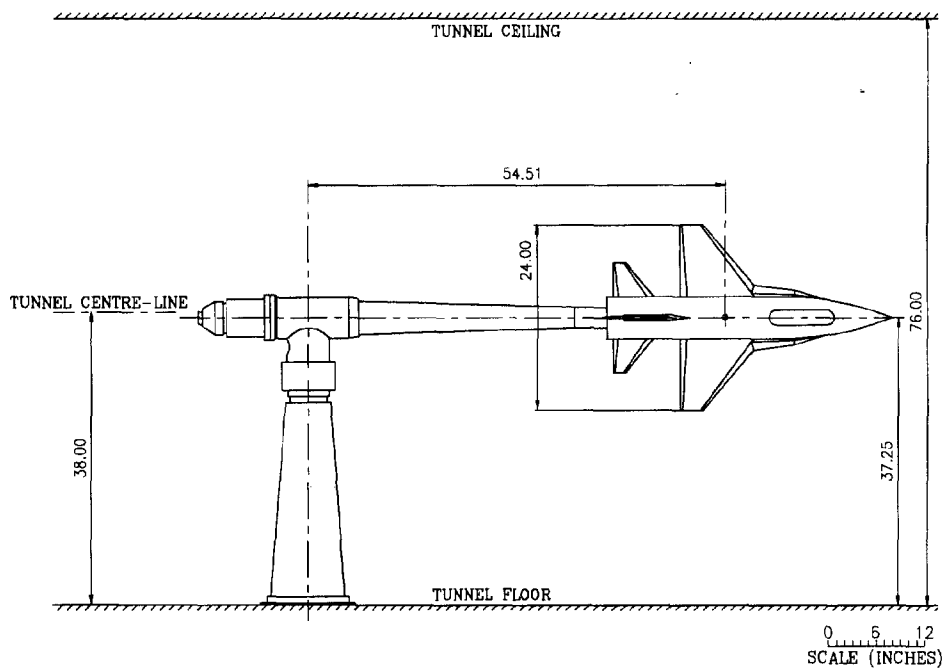


Fig 2 Side view of SDM-L model in the IAR 6 x 9 foot wind tunnel

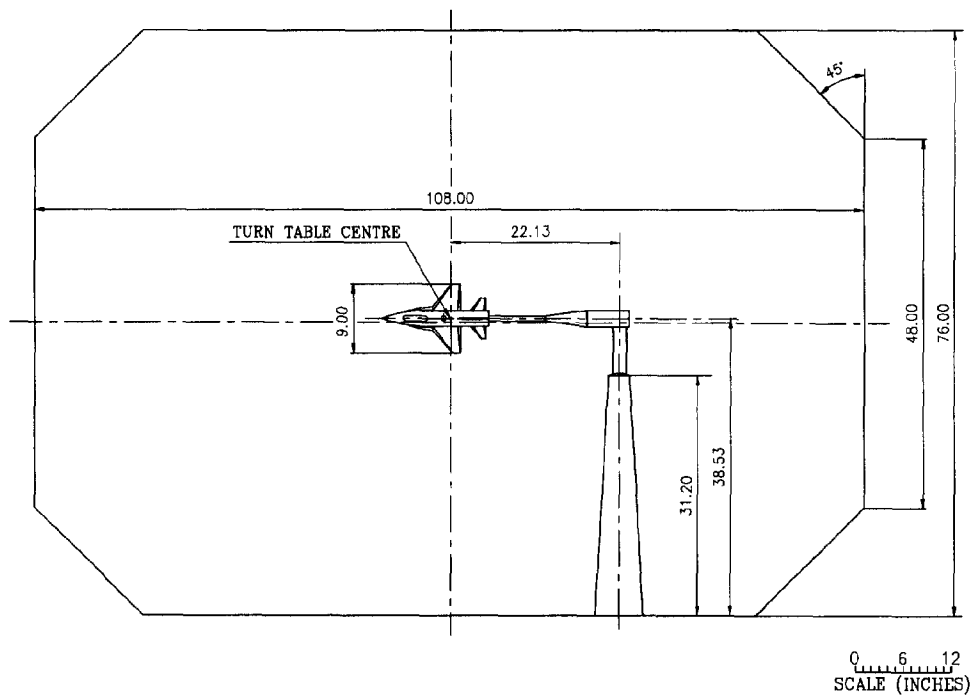


Fig. 3 Front view of SDM-S model in the IAR 6 x 9 foot wind tunnel

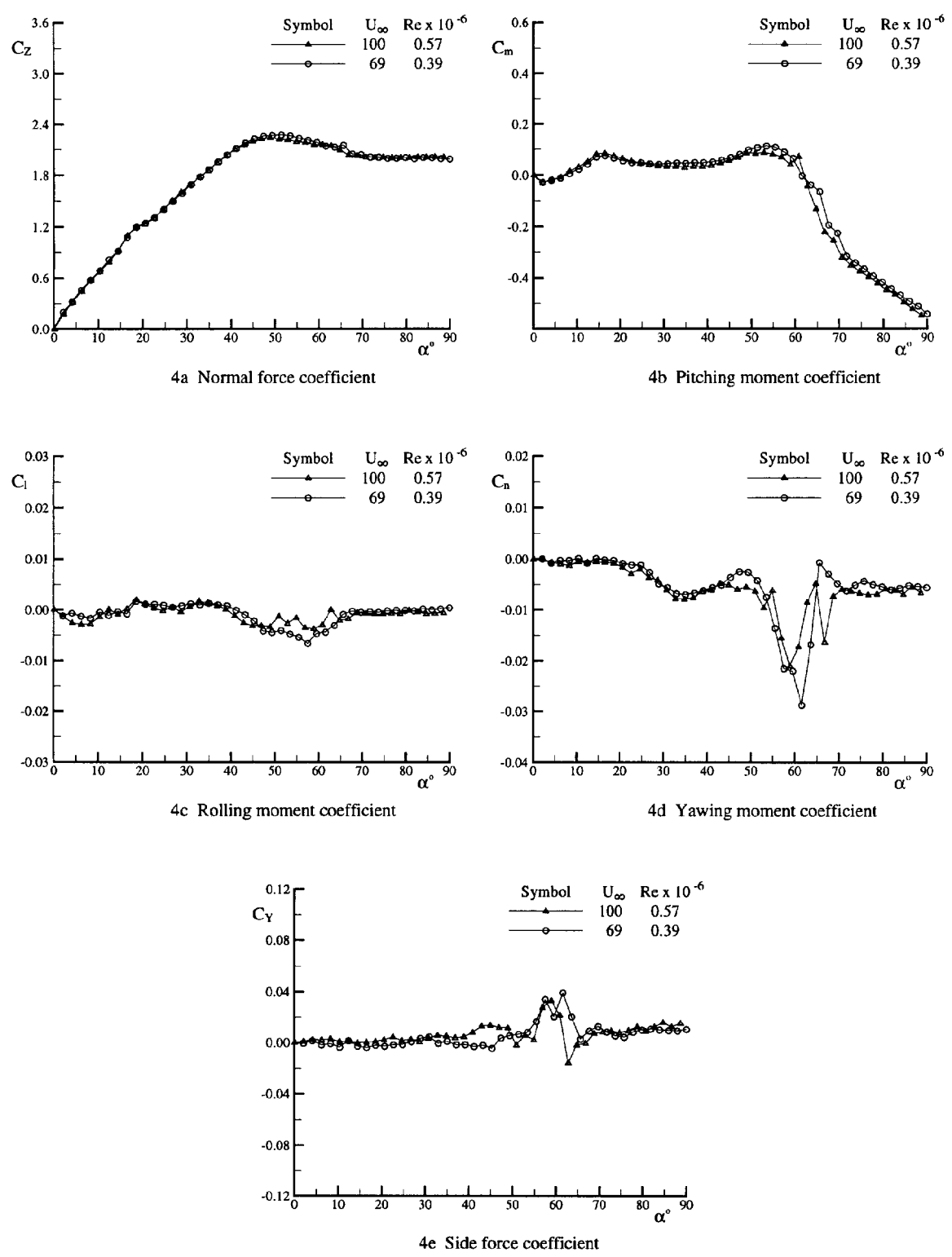
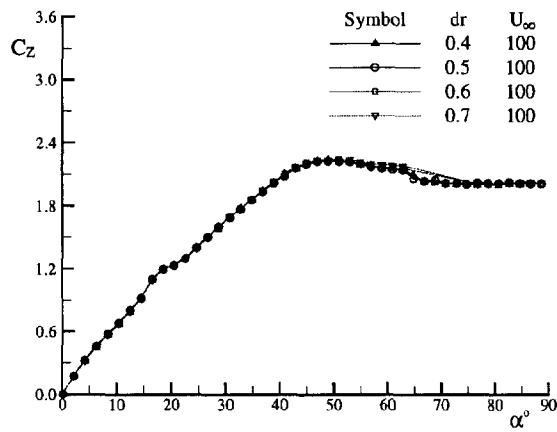
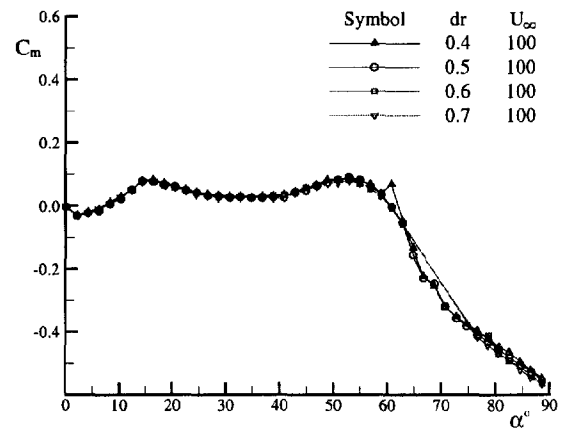


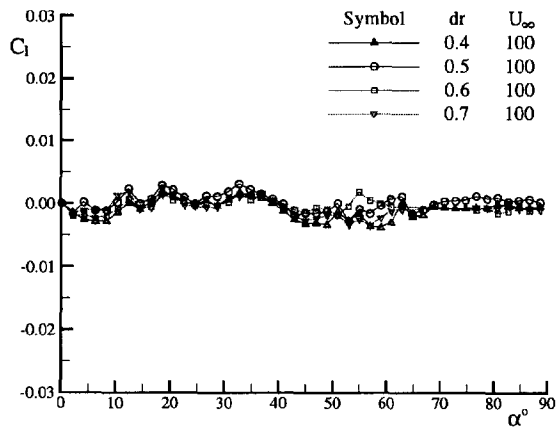
Fig. 4 Aerodynamic coefficients of SDM-S model at different velocities



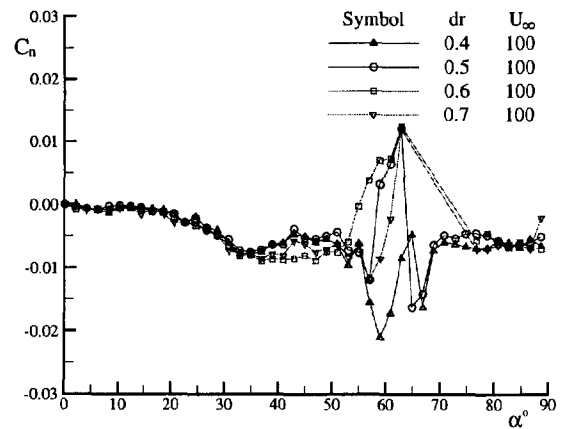
5a Normal force coefficient



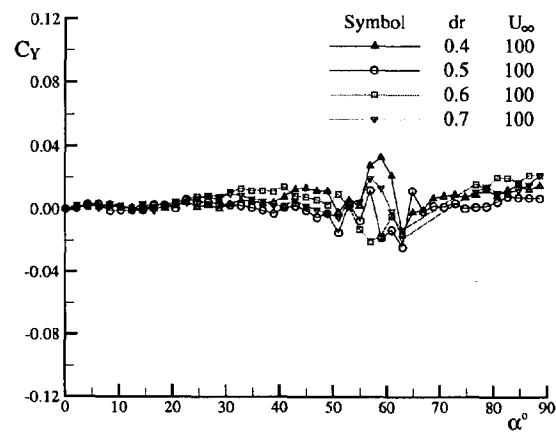
5b Pitching moment coefficient



5c Rolling moment coefficient



5d Yawing moment coefficient



5e Side force coefficient

Fig. 5 Aerodynamic coefficients of SDM-S model at different sting diameters

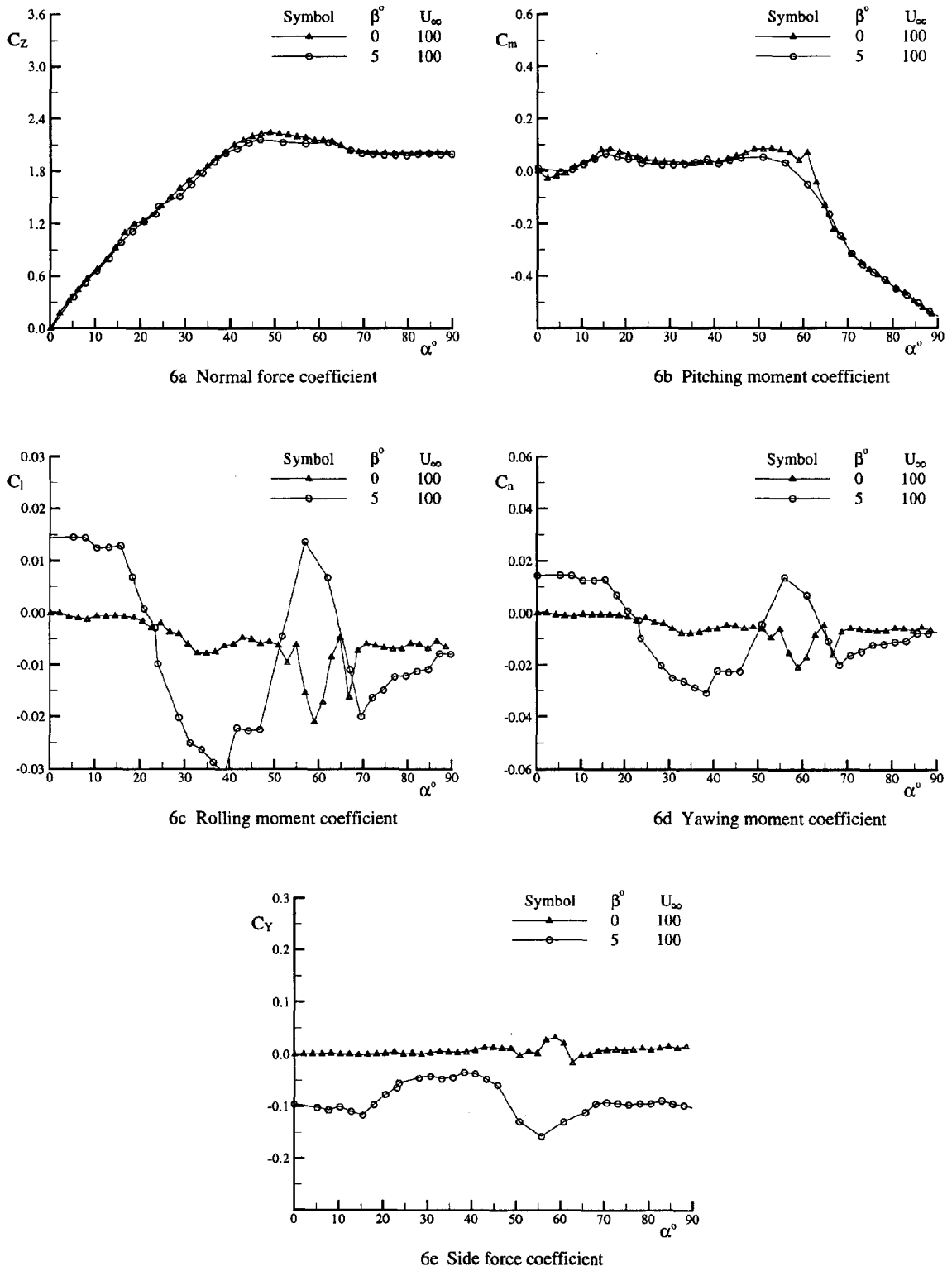
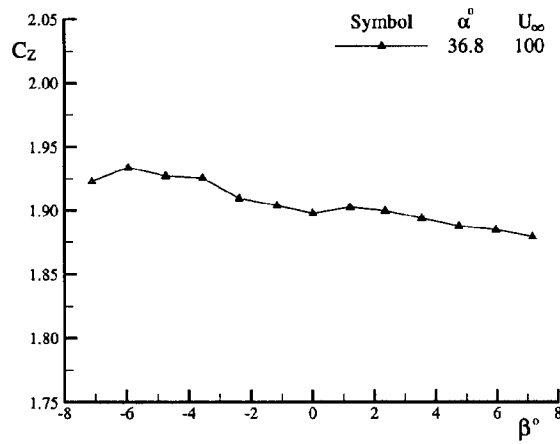
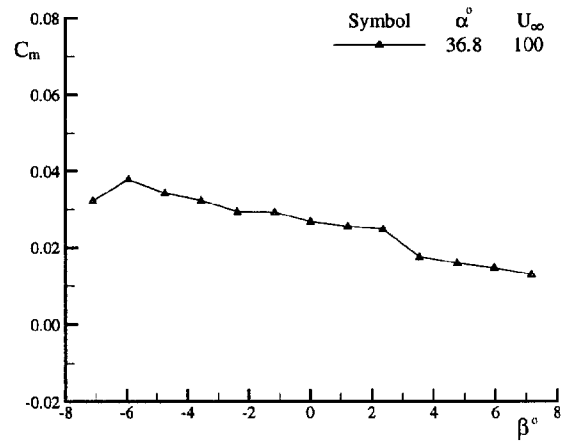


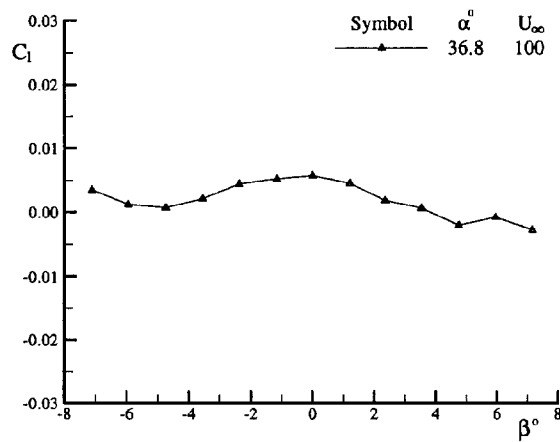
Fig. 6 Aerodynamic coefficients of SDM-S model at different sideslip angles



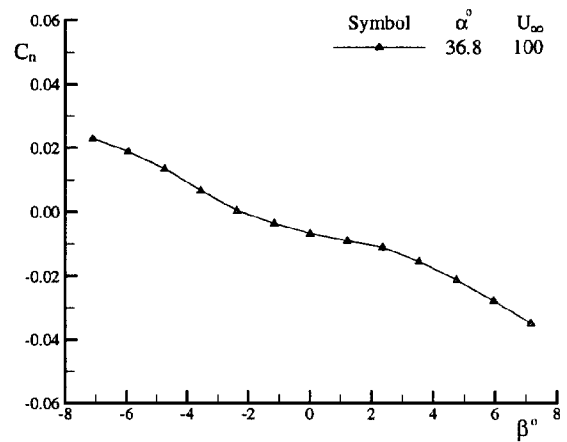
6f Normal force coefficient



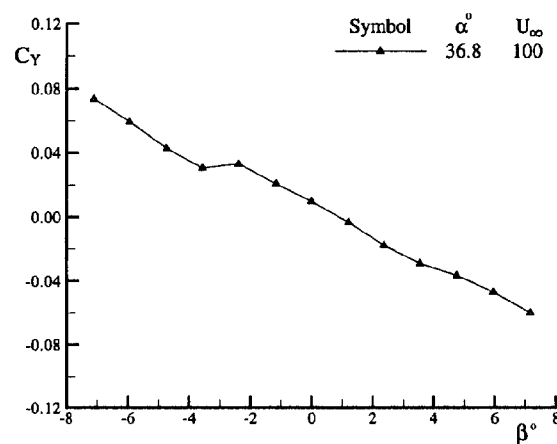
6g Pitching moment coefficient



6h Rolling moment coefficient



6i Yawing moment coefficient



6j Side force coefficient

Fig. 6(cont.) Aerodynamic coefficients of SDM-S model at different sideslip angles

Finite-element analysis

Measured results

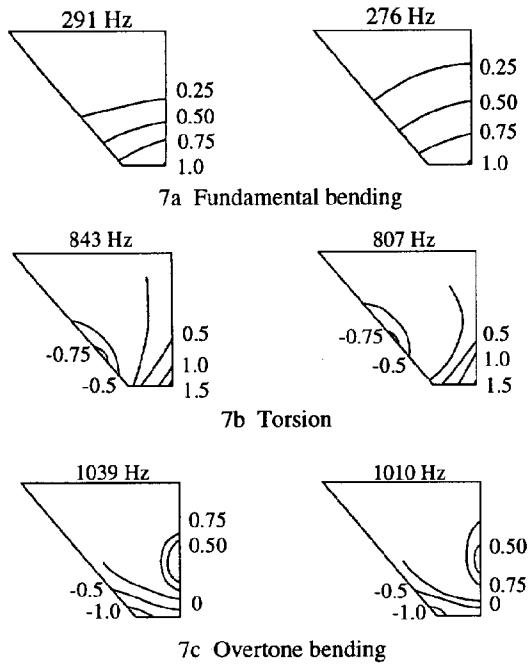


Fig. 7 Single-wing mode shapes

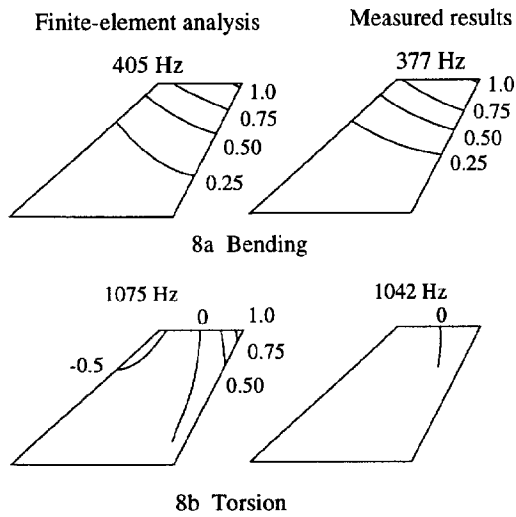


Fig. 8 Vertical fin mode shapes

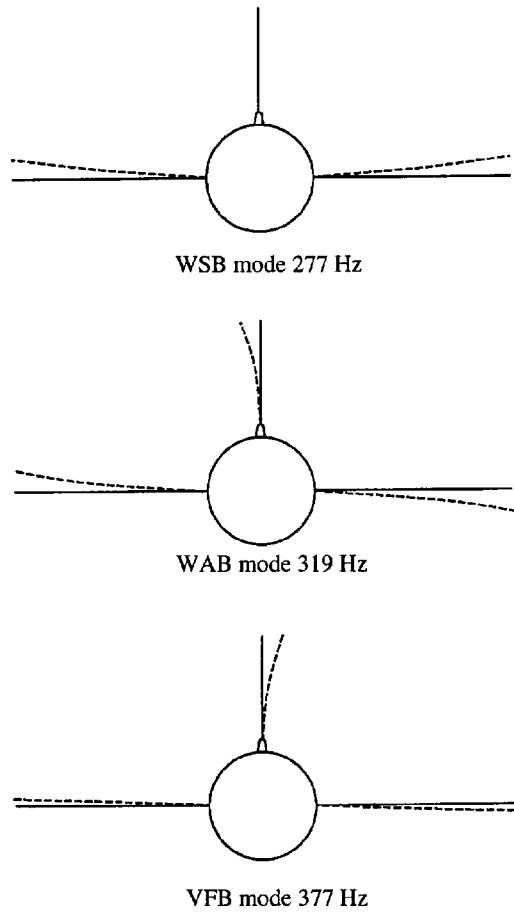


Fig. 9 Complete model modes

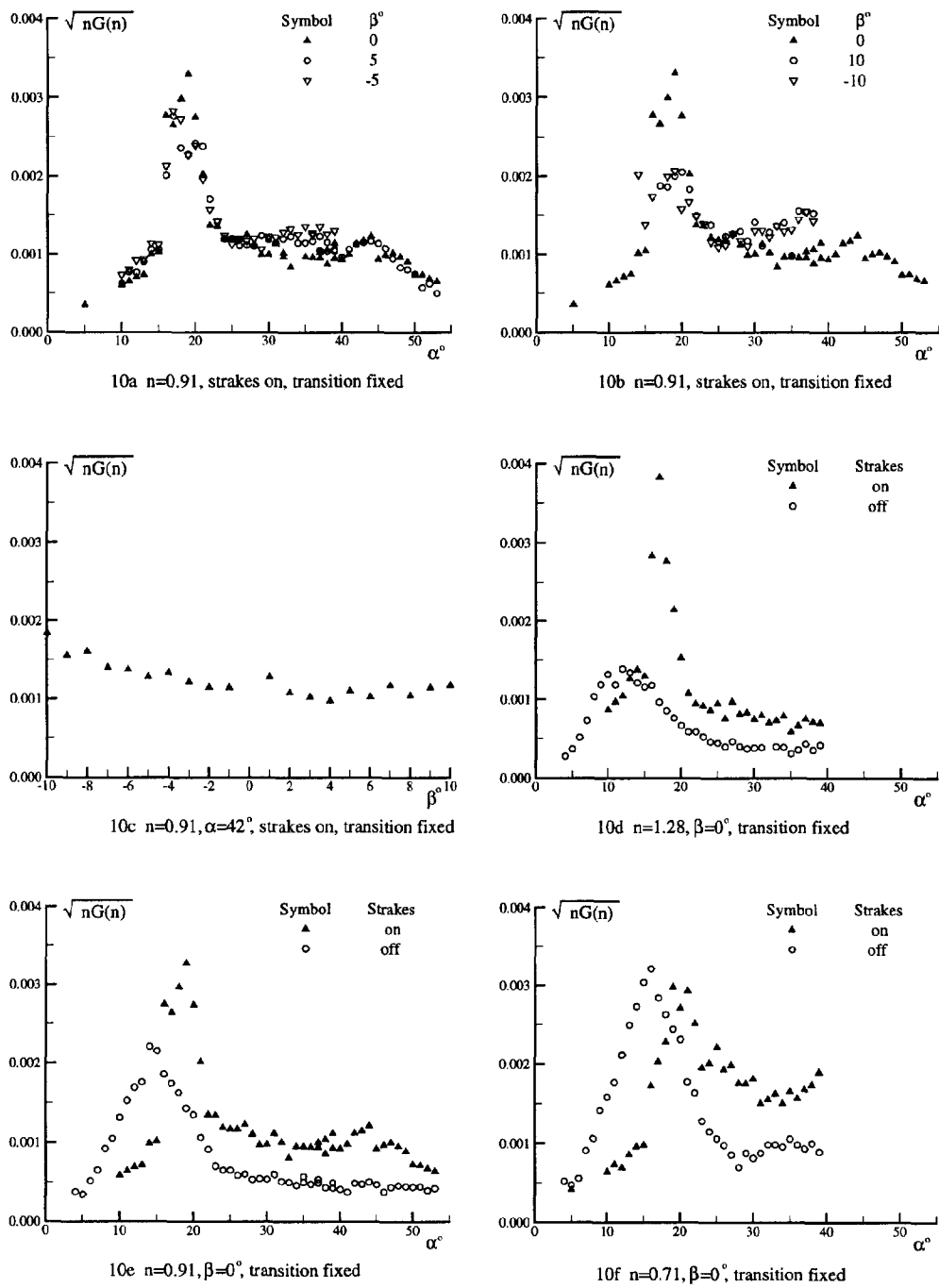


Fig. 10 Wing buffet excitation parameter of SDM-L model at different conditions (WSB mode)

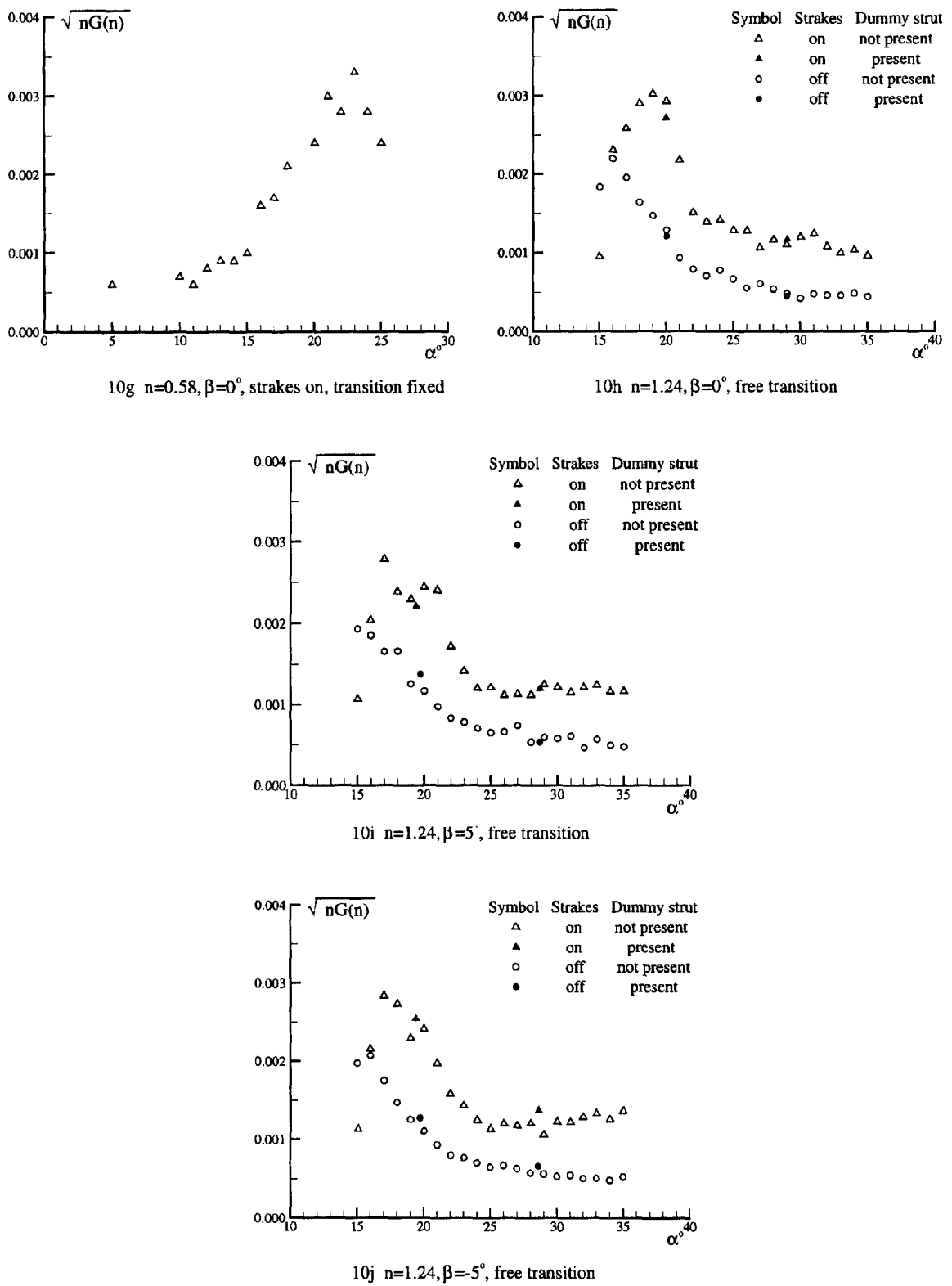


Fig. 10(cont.) Wing buffet excitation parameter of SDM-L model at different conditions (WSB mode)

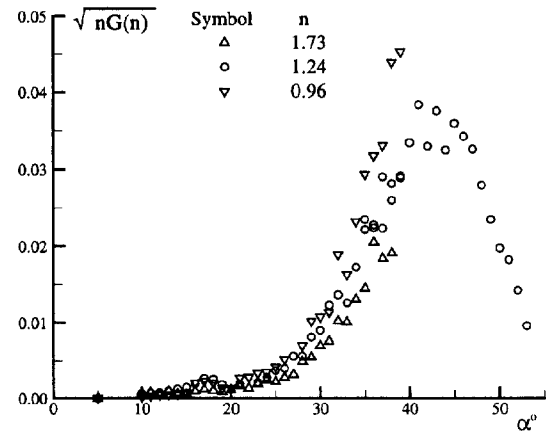
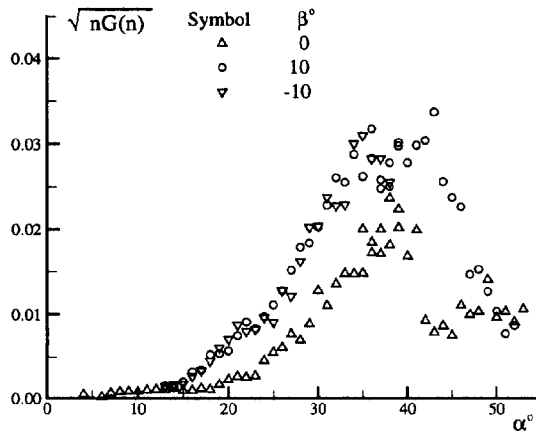
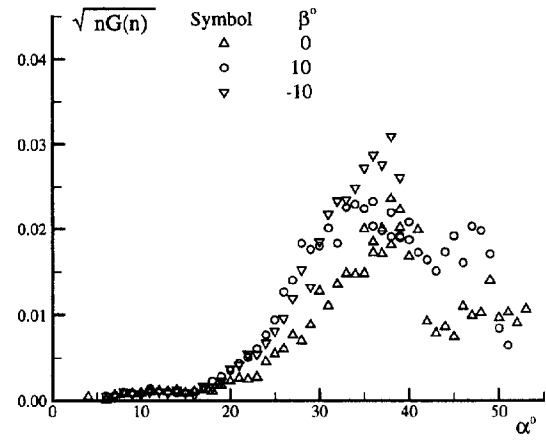
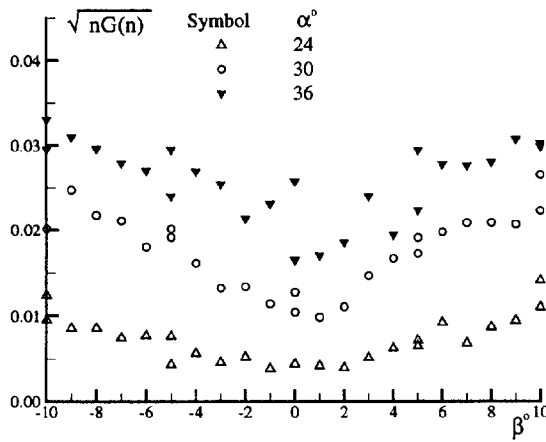
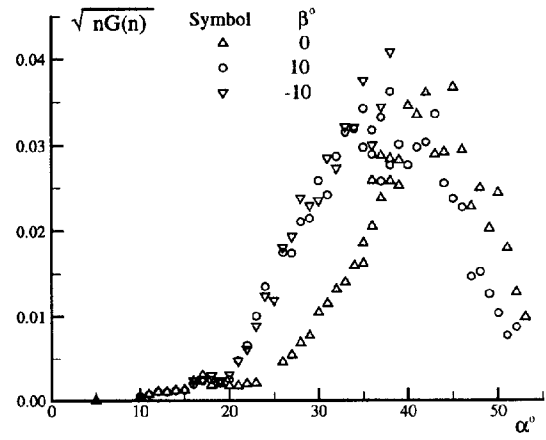
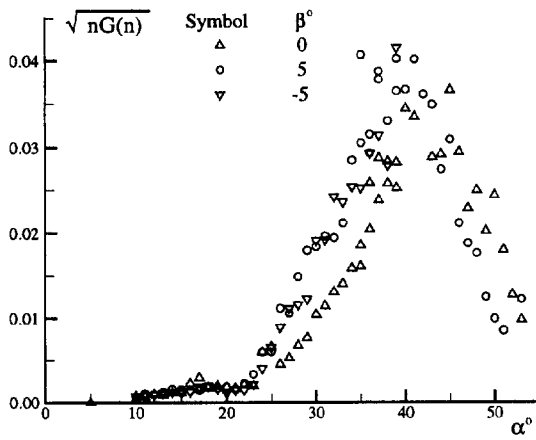


Fig. 11 Fin buffet excitation parameter of SDM-L model at different conditions (FVB mode)

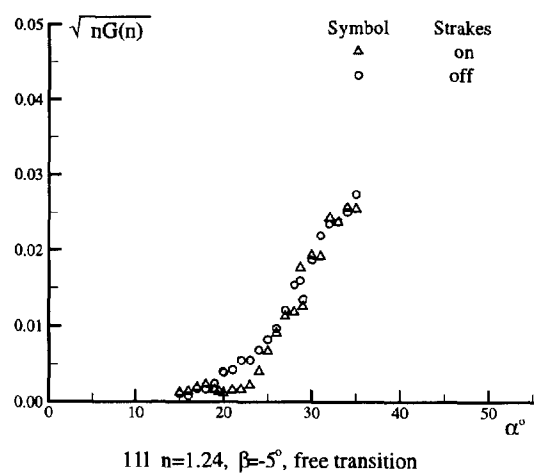
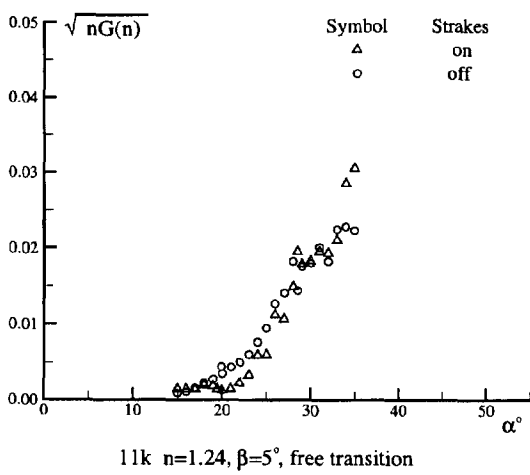
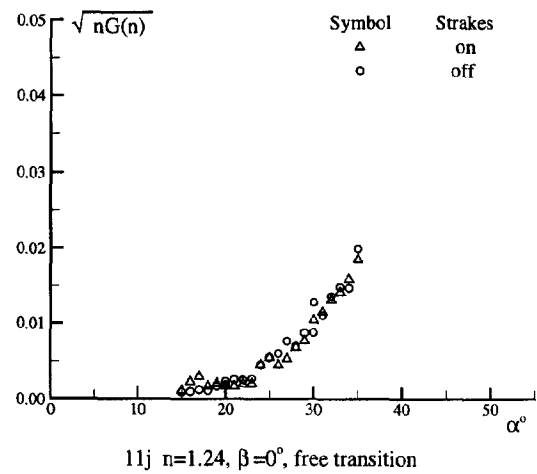
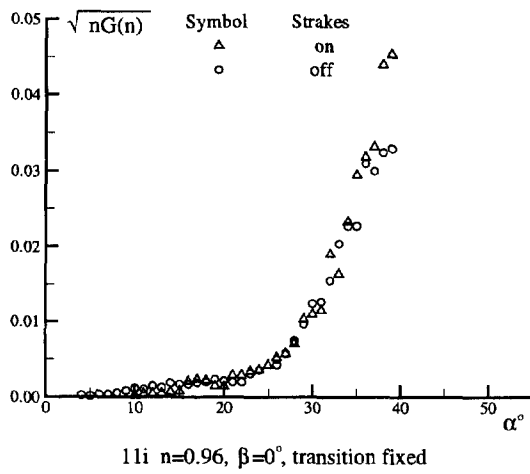
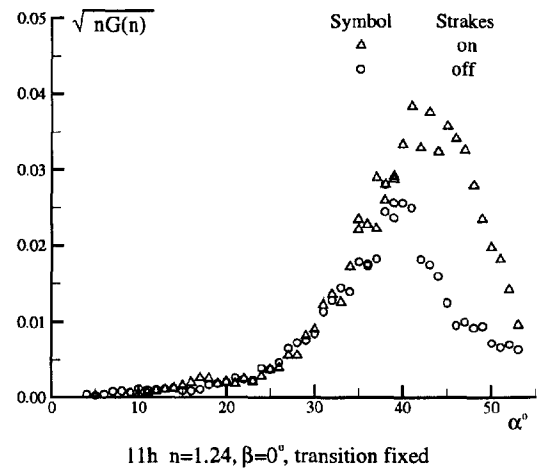
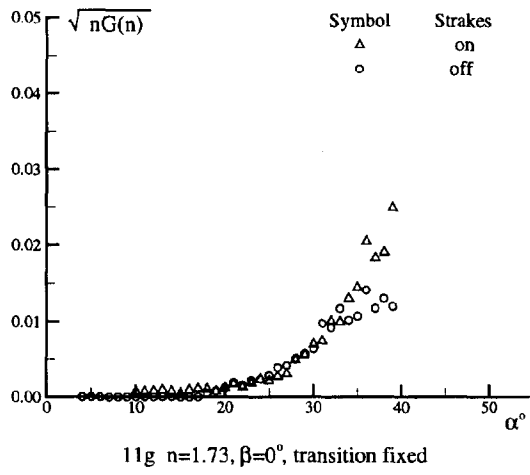
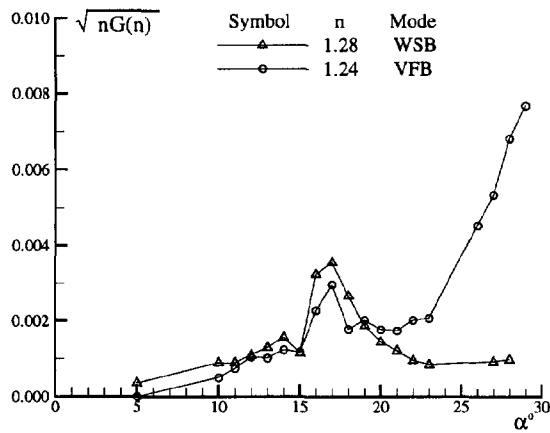
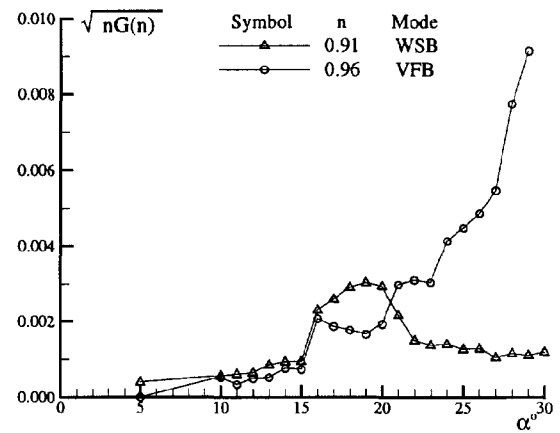
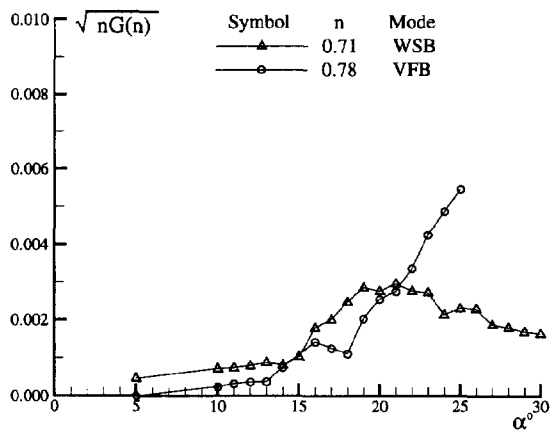
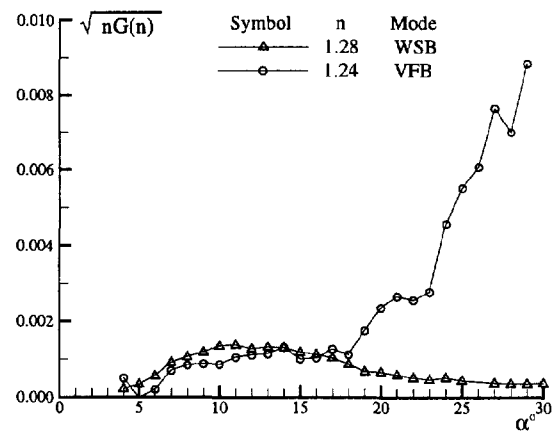
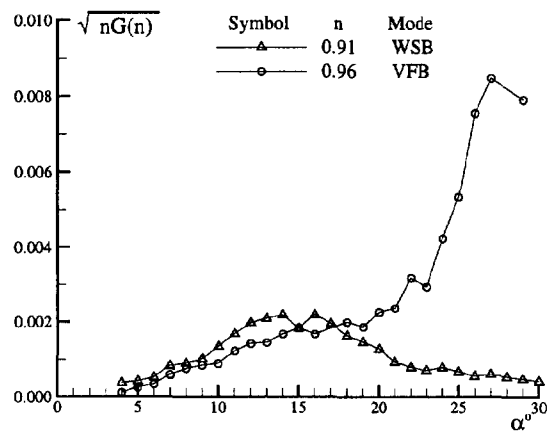


Fig.11(cont.) Fin buffet excitation parameter of SDM-L model at different conditions (FVB mode)

12a $n=1.28, 1.24$, strokes on12b $n=0.91, 0.96$, strokes on12c $n=0.71, 0.78$, strokes on12d $n=1.28, 1.24$, strokes off12e $n=0.91, 0.96$, strokes offFig. 12 Comparison of wing and fin buffet excitation ($\beta=0^\circ$, free transition)

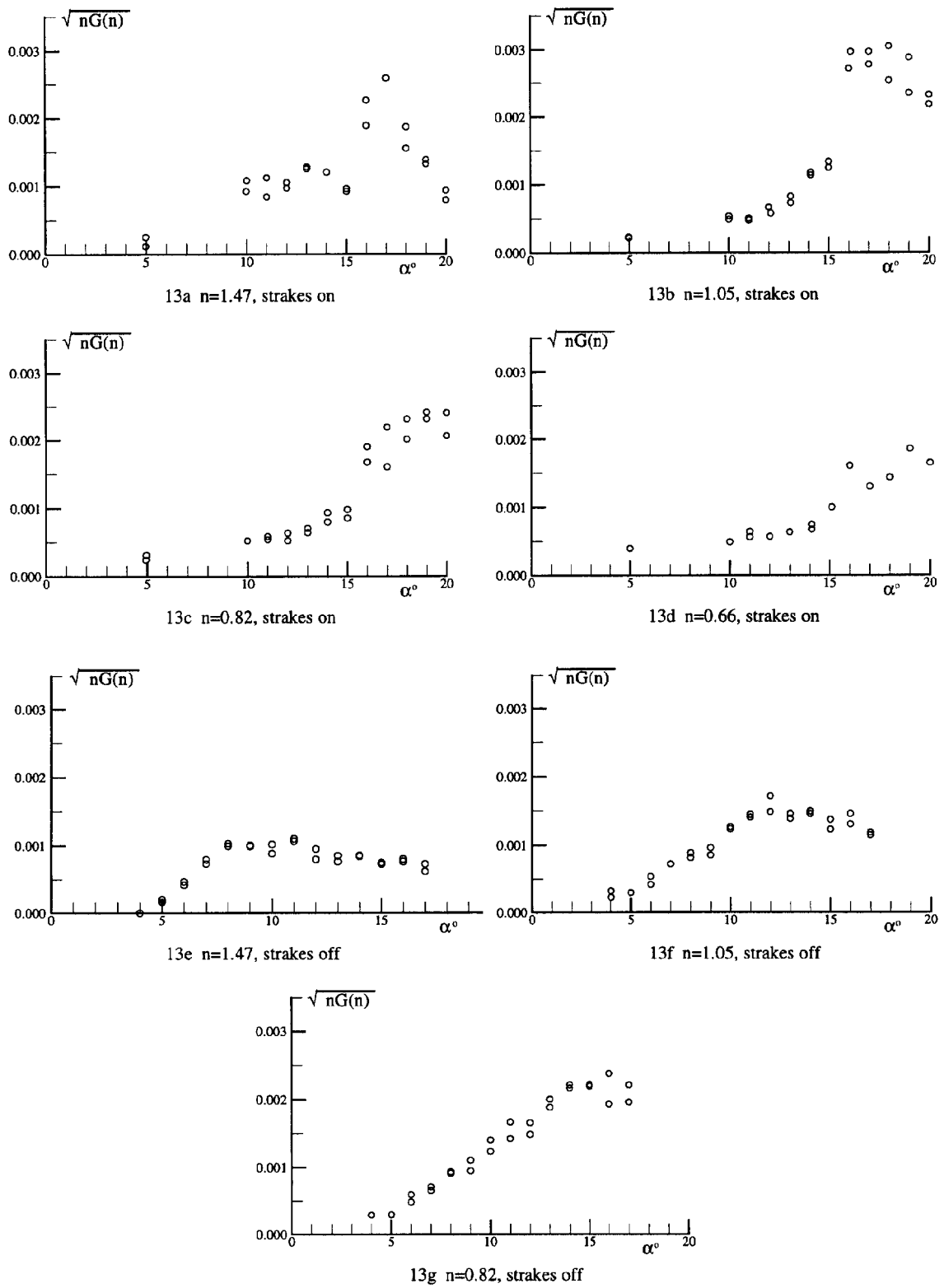


Fig. 13 Wing buffet excitation parameter of SDM-L model at different conditions (WAB mode, $\beta=0^\circ$)

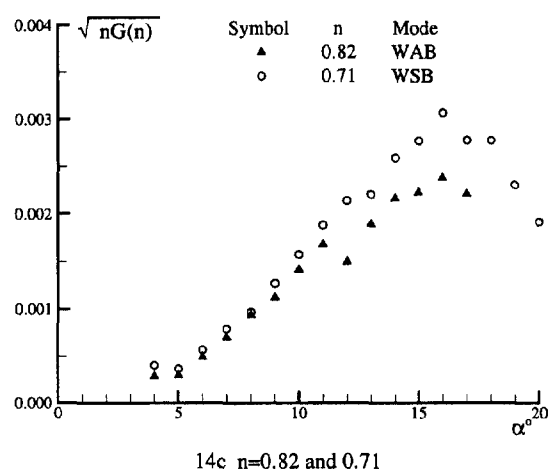
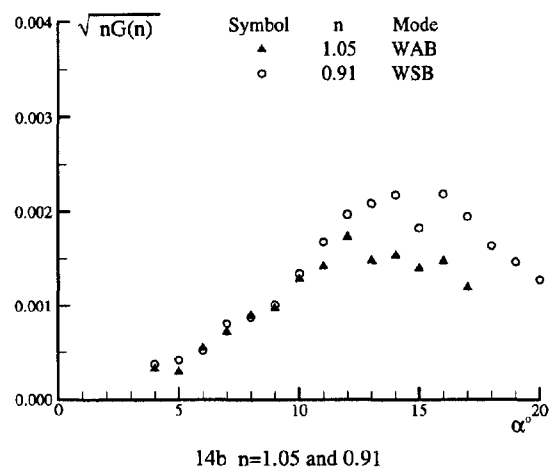
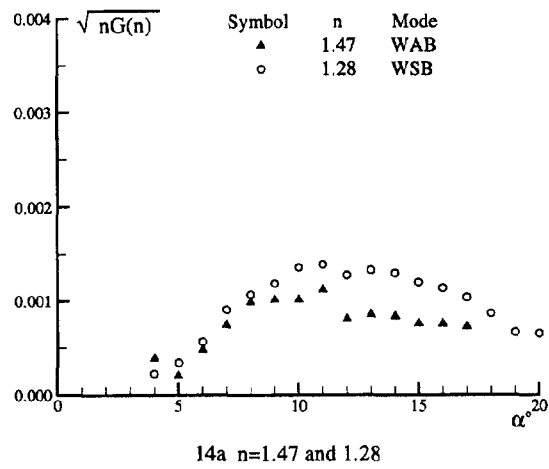


Fig. 14 Model independence on wing buffet excitation of SDM-L model (strakes off, $\beta=0^\circ$, free transition)

